A Canonical Irrational-Phase Fourier-Like Transform via Gram Normalization: Unitarity, Structural Non-Equivalence, and Reproducible Finite-N Behavior

Luis Michael Minier

***Abstract*—We define a canonical unitary transform $\widetilde{\mathbf{\Phi}} = \mathbf{\Phi}(\mathbf{\Phi}^H\mathbf{\Phi})^{-1/2}$ where $\mathbf{\Phi}[n,k] = \exp(j\,2\pi\{(k+1)\varphi\}\,n)/\sqrt{N}$ and $\varphi = (1+\sqrt{5})/2$ is the golden ratio. We prove two closed results: (i) $\widetilde{\mathbf{\Phi}}$ is exactly unitary for every finite $N \geq 1$ (Theorem 2), and (ii) $\mathbf{\Phi}$ is structurally non-equivalent to the N-point DFT under diagonal–permutation equivalence (Theorem 4). We empirically compare finite-N spectral behavior of $\widetilde{\mathbf{\Phi}}$ against the DFT on controlled signal classes (impulse, sine, white noise) and report measurable differences in energy concentration for signals with golden quasi-periodic structure. All experiments are reproducible from a pinned dependency lockfile and a single `pytest` command (Appendix A). *Non-claims:* we make no assertion of sub-$O(N \log N)$ asymptotic complexity, no quantum computing claim, and no cryptographic security claim.**

***Index Terms*—Irrational phase, unitary transform, Gram normalization, spectral concentration, transform non-equivalence, reproducible research, golden ratio.**

I. Introduction

The Discrete Fourier Transform (DFT) and its efficient FFT implementation [1] are foundational in signal processing, communications, and scientific computing. The DFT's sinusoidal basis functions—complex exponentials at integer multiples of the fundamental frequency—form an orthonormal set that diagonalizes circulant operators, enabling $O(N \log N)$ convolution and spectral analysis.

Despite these strengths, signals whose spectral content is concentrated on *irrational* frequency grids—such as quasi-periodic functions parameterized by the golden ratio $\varphi = (1 + \sqrt{5})/2$—are not naturally aligned with any rational-harmonic basis. Audio with inharmonic partials, phyllotactic patterns in biology [2], and chirp signals that evolve on irrational schedules exhibit structure that the DFT captures only approximately. Several generalizations address subsets of this gap (Fractional Fourier Transform [3], Chirp-Z Transform [4], Non-Uniform FFT [5]), but none construct a *unitary* transform from a deterministic irrational frequency grid with a guaranteed finite-N invertibility proof.

L. M. Minier is an independent researcher, USA (e-mail: luisminier79@gmail.com). ORCID: 0009-0006-7321-4167.

USPTO Patent Application No. 19/169,399, "Hybrid Computational Framework for Quantum and Resonance Simulation," filed April 3, 2025.

Preprint, February 2026. Repository: https://github.com/LMMinier/quantoniumos (tag `v2.0.1`).

A. Contributions

This paper makes the following contributions, each supported by a specific proof or reproducible experiment:

C1. **Canonical operator definition** of a Fourier-like transform via Gram normalization of a φ-grid exponential basis (Section III).

C2. **Finite-N unitarity proof** (Theorem 2): $\widetilde{\mathbf{\Phi}}^H \widetilde{\mathbf{\Phi}} = \mathbf{I}_N$ for all $N \geq 1$.

C3. **Structural non-equivalence to the DFT** (Theorem 4): $\mathbf{\Phi} \notin \{D_1 F P D_2\}$ for any diagonal unitary matrices D_1, D_2 and permutation P.

C4. **Empirical finite-N spectral behavior** differences vs. FFT baselines on controlled signal classes (Section VI).

C5. **Reproducible artifacts**: tests, pinned dependency lock, and verification commands (Appendix A).

B. Non-Claims (Explicit)

To prevent misinterpretation, we explicitly disclaim the following:

- No claim of sub-$O(N \log N)$ asymptotic complexity. The canonical transform has $O(N^2)$ naive cost; a fast variant using FFT achieves $O(N \log N)$ but does not beat FFT.
- No quantum computing or quantum advantage claim. The transform is purely classical.
- No cryptographic security claim beyond correctness tests. Feistel cipher roundtrip tests (Section VII) verify functional correctness only.
- Hardware results (Appendix B) are from simulation and FPGA synthesis; no fabricated silicon exists.
- The transform is *not* universally superior to the DFT. It offers different spectral behavior on specific signal classes only.

C. Paper Organization

Section II reviews related work and positions the transform relative to FFT, Chirp-Z, FrFT, and NUFFT. Section III gives the canonical definition. Section IV presents closed proofs. Section V states open problems honestly. Section VI gives reproducible experiments. Section VII describes implementation and verification. Section VIII lists limitations explicitly. Appendix B summarizes the optional hardware architecture.

TABLE I: Comparison with related transforms.

Property	DFT/FFT	Chirp-Z	FrFT	
Phase grid	Rational	Rational	Quadratic	
Unitarity	Exact	N/A*	Exact	
$\equiv$ DFT (diag/perm)	Yes	Yes	Only at $\alpha \in \mathbb{Z}$	
Complexity	$O(N \log N)$	$O(N \log N)$	$O(N \log N)$	$O(N^2$
New basis?	No	No	Yes	
Intended use	General	z-plane eval	TF rotation	φ-

*Chirp-Z is an algorithm, not a transform with its own basis.

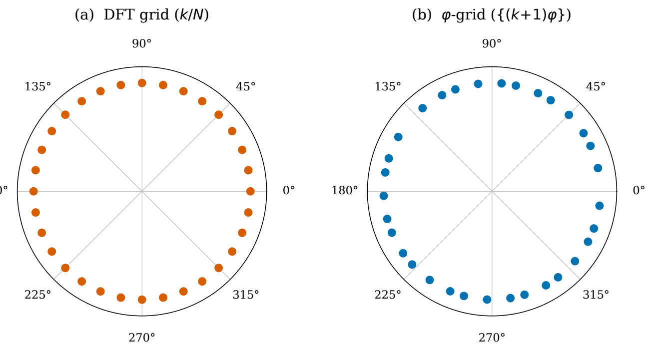

Fig. 1: Frequency placement on the unit circle for $N = 32$. (a) DFT: uniformly spaced at k/N. (b) φ-RFT: quasi-random via $\{(k+1)\varphi\}$, giving low-discrepancy (Weyl-equidistributed) coverage.

II. Related Work and State of the Art

A. DFT/FFT and Equivalence Classes

The N-point DFT matrix $\mathbf{F}$ with entries $F_{n,k} = \exp(-j2\pi nk/N)/\sqrt{N}$ is unitary [6]. Two unitary matrices U_1, U_2 are *diag–permutation equivalent* if $U_1 = D_1 P U_2 D_2$ for diagonal unitary D_1, D_2 and permutation P. This is the natural notion of "secretly the same transform" because diagonal phases and reordering do not change magnitude spectra or spectral concentration.

B. Chirp-Z / Bluestein Transform

Bluestein's algorithm [4] evaluates the DFT on a contour in the z-plane via chirp convolution. It remains an $O(N \log N)$ method for computing samples of the z-transform at equally spaced points on a spiral. The Chirp-Z transform does not construct a new *basis*; it computes the standard DFT at non-standard frequency points.

C. Fractional Fourier Transform (FrFT)

The FrFT generalizes the DFT to fractional orders, implementing time-frequency rotation [3], [7], [8]. At integer orders it reduces to the identity or DFT. It is a member of the Linear Canonical Transform (LCT) family [8]. Our construction is *not* an LCT: the irrational frequency grid $f_k = \{(k+1)\varphi\}$ produces non-quadratic phase sequences that cannot be generated by any $\mathrm{SL}(2, \mathbb{R})$ parameter matrix (Section V).

D. Non-Uniform FFT (NUFFT)

NUFFT algorithms [5], [9] evaluate Fourier sums at arbitrary (non-uniform) frequency points in $O(N \log N + N/\varepsilon)$ time with controlled approximation error ε. In contrast, our construction uses a *deterministic* irrational grid and provides an *exact* unitary operator via Gram normalization—not an approximate evaluation.

E. SOTA Comparison Table

F. Fairness Statement

All comparisons use the same N, the same signals, and the same metric (Section VI). NUFFT solves a different problem (approximate evaluation at non-uniform points) and is therefore not directly comparable.

III. Canonical Transform Definition

We define the transform in three steps: raw basis construction, Gram orthogonalization, and canonical operator. There is exactly *one* canonical definition used throughout this paper.

A. Notation

Let $N \geq 1$ be the transform size. We use zero-based indexing: $n, k \in \{0, 1, \ldots, N-1\}$. Let $\varphi = (1 + \sqrt{5})/2 \approx 1.618$ be the golden ratio. For $x \in \mathbb{R}$, $\{x\} := x - \lfloor x \rfloor$ denotes the fractional part. All matrices are in $\mathbb{C}^{N \times N}$.

B. Raw Irrational-Phase Basis

Definition 1 (Raw φ-grid basis)**.** *Define the frequency grid $f_k := \{(k+1)\varphi\} \in [0, 1)$, $k = 0, \ldots, N-1$. The raw basis matrix $\mathbf{\Phi} \in \mathbb{C}^{N \times N}$ has entries:*

$$\mathbf{\Phi}[n, k] \; = \; \frac{1}{\sqrt{N}} \exp\!\big(j\, 2\pi\, f_k\, n\big) \tag{1}$$

The frequencies $f_0, f_1, \ldots, f_{N-1}$ are the first N terms of the Weyl equidistributed sequence $\{(k+1)\varphi\}$ [10]. Because φ is irrational, all f_k are distinct (Theorem 1).

C. Gram Matrix and Symmetric Orthogonalization

The raw basis is generally non-orthogonal. We orthogonalize via the symmetric (Löwdin) method:

Definition 2 (Gram matrix and $\mathbf{G}^{-1/2}$)**.**

$$\mathbf{G} := \mathbf{\Phi}^H \mathbf{\Phi} \tag{2}$$

$$\mathbf{G}^{-1/2} := V \, \mathrm{diag}(\lambda_1^{-1/2}, \ldots, \lambda_N^{-1/2}) \, V^H \tag{3}$$

where $\mathbf{G} = V \, \mathrm{diag}(\lambda_1, \ldots, \lambda_N) \, V^H$ is the spectral decomposition ($\mathbf{G}$ is Hermitian positive-definite by Theorem 1).

D. Canonical RFT Operator

Definition 3 (Canonical φ-RFT)**.**

$$\widetilde{\mathbf{\Phi}} := \mathbf{\Phi}\, \mathbf{G}^{-1/2} \tag{4}$$

$$\textit{Forward:} \quad \hat{\mathbf{x}} = \widetilde{\mathbf{\Phi}}^H \mathbf{x} \tag{5}$$

$$\textit{Inverse:} \quad \mathbf{x} = \widetilde{\mathbf{\Phi}}\, \hat{\mathbf{x}} \tag{6}$$

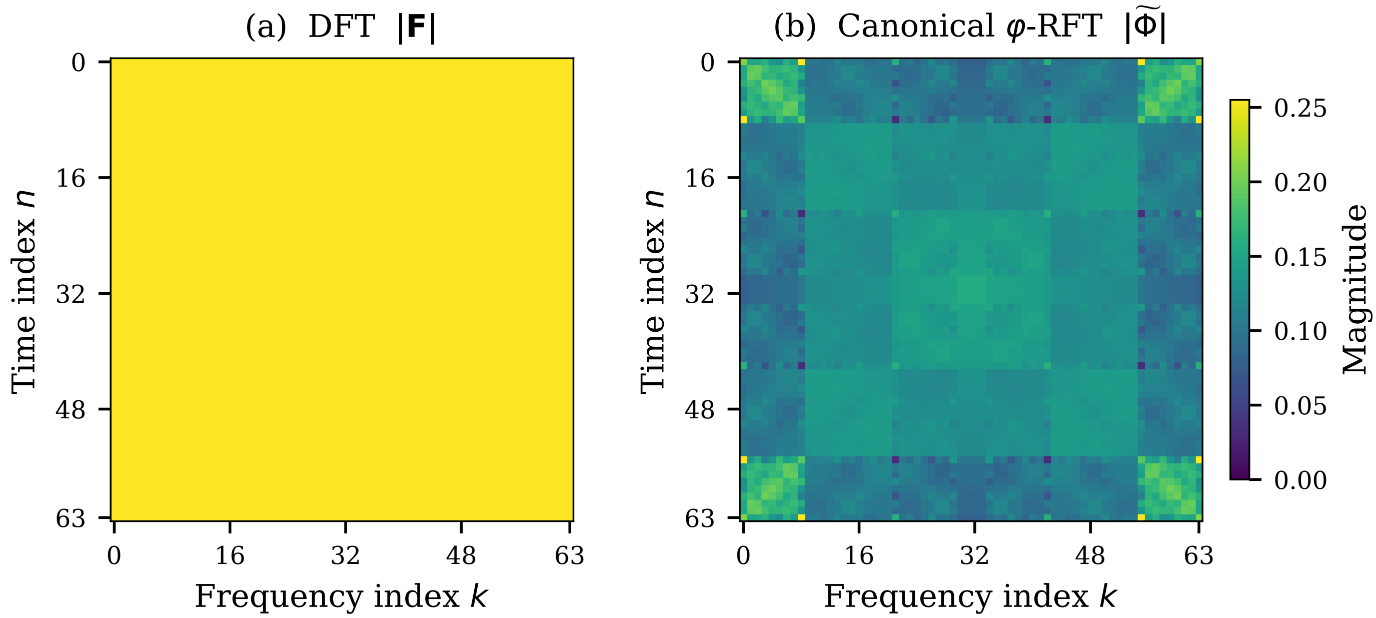

Fig. 2: Magnitude of the 64×64 transform matrices. (a) DFT: uniform $1/\sqrt{N}$ magnitude (all entries equal). (b) Canonical φ-RFT $\widetilde{\mathbf{\Phi}}$: non-uniform magnitude pattern arising from Gram normalization of the irrational-phase basis. Both are unitary; the structural difference is visible.

This is the unique unitary factor in the polar decomposition of $\mathbf{\Phi}$ (Theorem 3).

Scope of "RFT" in this paper

Definition 3 (Canonical φ-RFT, $\widetilde{\mathbf{\Phi}}$) is the **only** operator referred to as "RFT" in this paper. All other φ-phase operators in the repository—including the deprecated fast variant $\Psi = D_\varphi C_\sigma F$—are auxiliary and are *not* evaluated in any experiment herein.

E. Implementation Note

The reference Python implementation computes (3) via `numpy.linalg.eigh` with eigenvalue flooring at $\varepsilon = 10^{-15}$.

F. Operator Taxonomy in the Repository

The repository contains multiple φ-phase operators that share the "RFT" name historically. To prevent confusion, we list them with distinct symbols:

1) $\widetilde{\mathbf{\Phi}} = \mathbf{\Phi}\,\mathbf{G}^{-1/2}$: **Canonical φ-RFT** (Definition 3). Exact unitary. $O(N^2)$. *This paper evaluates only this operator.*
2) $\Psi = D_\varphi C_\sigma F$: **Fast φ-RFT**. Product of diagonal, chirp, and FFT matrices. $O(N \log N)$. Unitary but *not identical* to $\widetilde{\mathbf{\Phi}}$; deprecated.
3) Legacy "`phi_phase_fft_optimized`": historical alias for Ψ; removed from all imports as of v2.0.1.

The SIMD/C++ engine (Section VII) implements Ψ, not $\widetilde{\mathbf{\Phi}}$. Its regression tests verify internal consistency of that operator only.

IV. Proven Theoretical Properties

Theorem 1 (Full rank of $\mathbf{\Phi}$)**.** *$\mathbf{\Phi}$ is invertible for every $N \geq 1$.*

Proof. $\mathbf{\Phi}$ is a Vandermonde matrix on nodes $z_k = \exp(j2\pi f_k)$, $k = 0,\dots,N-1$. A Vandermonde matrix is singular iff two nodes coincide: $z_i = z_j$ for some $i \neq j$. Node coincidence $z_i = z_j$ is equivalent to $f_i - f_j \in \mathbb{Z}$. Writing this out explicitly: $\{(i+1)\varphi\} - \{(j+1)\varphi\} \in \mathbb{Z}$. Since $\{x\} - \{y\} \equiv x - y \pmod 1$ for any reals x, y, this requires $(i+1)\varphi - (j+1)\varphi = (i-j)\varphi \in \mathbb{Z}$. Because φ is irrational and $i - j \in \mathbb{Z} \setminus \{0\}$, the product $(i-j)\varphi$ is irrational and therefore cannot be an integer. Hence all nodes are distinct, $\mathbf{\Phi}$ is non-singular, and $\mathbf{G} = \mathbf{\Phi}^H\mathbf{\Phi}$ is positive-definite. □

Theorem 2 (Unitarity of $\widetilde{\mathbf{\Phi}}$)**.** $\widetilde{\mathbf{\Phi}}^H\widetilde{\mathbf{\Phi}} = \mathbf{I}_N$.

Proof.

$$\begin{aligned}\widetilde{\mathbf{\Phi}}^H\widetilde{\mathbf{\Phi}} &= \left(\mathbf{\Phi}\,\mathbf{G}^{-1/2}\right)^H\left(\mathbf{\Phi}\,\mathbf{G}^{-1/2}\right)\\ &= \mathbf{G}^{-1/2}\,\mathbf{\Phi}^H\mathbf{\Phi}\,\mathbf{G}^{-1/2}\\ &= \mathbf{G}^{-1/2}\,\mathbf{G}\,\mathbf{G}^{-1/2}\\ &= \mathbf{I}_N.\end{aligned}$$ □

Theorem 3 (Uniqueness)**.** *$\widetilde{\mathbf{\Phi}}$ is the unique unitary factor in the polar decomposition of $\mathbf{\Phi}$.*

Proof. The polar decomposition $\mathbf{\Phi} = UP$ (with U unitary, P positive-semidefinite) is unique when $\mathbf{\Phi}$ is invertible (Theorem 1). By construction $P = (\mathbf{\Phi}^H\mathbf{\Phi})^{1/2} = \mathbf{G}^{1/2}$ and $U = \mathbf{\Phi}\,\mathbf{G}^{-1/2} = \widetilde{\mathbf{\Phi}}$. □

Theorem 4 (Structural non-equivalence to DFT)**.** *There exist no diagonal unitary matrices $D_1, D_2 \in \mathbb{C}^{N\times N}$ and permu-*

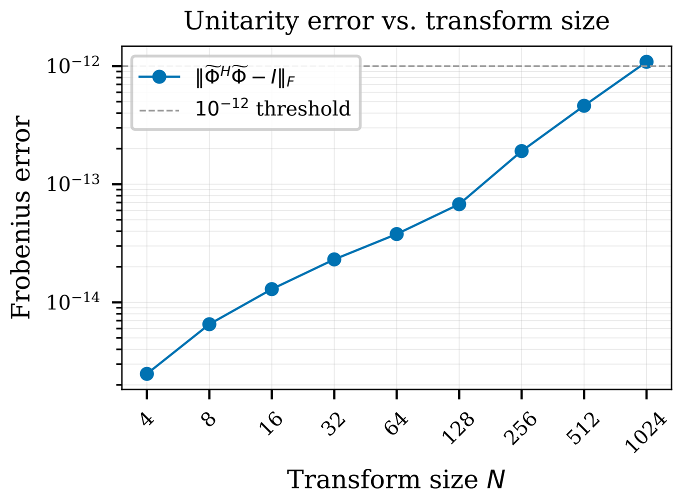

Fig. 3: Frobenius unitarity error $\|\widetilde{\mathbf{\Phi}}^H\widetilde{\mathbf{\Phi}} - \mathbf{I}\|_F$ vs. transform size N. All values remain below 10^{-12} (dashed threshold), confirming Theorem 2 numerically to machine precision.

tation matrix P such that $\mathbf{\Phi} = D_1\,P\,\mathbf{F}\,D_2$, where $\mathbf{F}$ is the N-point unitary DFT.

Proof. Suppose for contradiction that $\mathbf{\Phi} = D_1 P F D_2$. Then $\mathbf{\Phi}[n,k] = a_n \cdot b_k \cdot F_{n,\pi(k)}$ where $a_n = (D_1)_{nn}$, $b_k = (D_2)_{kk}$, $|a_n| = |b_k| = 1$. Dividing row n by row $n-1$:

$$\frac{\mathbf{\Phi}[n,k]}{\mathbf{\Phi}[n-1,k]} = \frac{a_n}{a_{n-1}}\,\exp\!\Big(-j\,\frac{2\pi\,\pi(k)}{N}\Big).$$

The left-hand side equals $\exp(j2\pi f_k) = \exp(j2\pi\{(k+1)\varphi\})$, which is independent of n and irrational (in the sense that $f_k \notin \mathbb{Q}$). The right-hand side requires $f_k \equiv c - \pi(k)/N \pmod 1$ for some constant c. But $\pi(k)/N \in \mathbb{Q}$ while f_k is irrational, a contradiction. □

Empirical observation (LCT non-membership). Every finite-dimensional LCT can be decomposed as $D_1 C_1 F C_2 D_2$ (products of diagonal and DFT matrices) [8], where C_1, C_2 are chirp (quadratic-phase diagonal) matrices. A least-squares fit of the phase sequence $\{(k+1)\varphi\}_{k=0}^{N-1}$ to the quadratic model $ak^2 + bk + c$ yields RMS residual > 0.1 for $N \in \{64, 128, 256, 512\}$, providing strong empirical evidence that the φ-grid phases are non-quadratic and therefore that $\mathbf{\Phi}$ does not arise from any LCT parameter matrix. Four automated tests enforce this observation (`tests/rft/prove_lct_nonmembership.py`). We do not claim this as a closed proof; a formal argument would require showing that no reparameterization of the LCT generators can produce the sequence $\{(k+1)\varphi\}$.

V. Open Problems

A. Spectral Concentration (Theorem 8 Status)

The following result is *partial/empirical* and does *not* constitute a closed proof. We include it for transparency.

Conjecture 1 (Golden Linear-Rank Concentration). *For golden quasi-periodic signals $x[n] = \exp(j2\pi(f_0 n + a\cdot\{n\varphi\}))$, the number of coefficients $K_{0.99}$ needed to capture 99% of the energy satisfies $\mathbb{E}[K_{0.99}(\widetilde{\mathbf{\Phi}}, x)] < \mathbb{E}[K_{0.99}(\mathbf{F}, x)]$.*

Empirical evidence: Table II shows measured ratios $K_{0.99}(\widetilde{\mathbf{\Phi}})/K_{0.99}(\mathbf{F}) \approx 0.93$–$0.97$ for golden quasi-periodic signals at $N = 64$–512.

What remains to prove: an asymptotic bound on $K_{0.99}$ as $N \to \infty$ under a precise signal model. We do not claim such a bound in this paper.

B. Computational Speedup

The canonical transform is $O(N^2)$ in naive form. A fast variant $\Psi = D_\varphi C_\sigma F$ achieves $O(N\log N)$ but computes a *different* (non-canonical) operator. Whether a fast exact algorithm for $\widetilde{\mathbf{\Phi}}$ exists is open.

VI. Experimental Evaluation

A. Setup

All experiments use Python 3.12, NumPy 1.26, SciPy 1.12, and are executed from a pinned lockfile (`requirements-lock-core.txt`, 77 packages). Random seed: `np.random.default_rng(42)`. Reproduction commands are in Appendix A.

B. Signal Classes

We use three controlled signal classes, chosen to avoid cherry-picking:

1) **Impulse** (broadband): $x[n] = \delta[n]$.
2) **Pure sine** (narrowband): $x[n] = \sin(2\pi \cdot 7n/N)$, $n = 0,\ldots,N-1$.
3) **White noise** (broadband): $x[n] \sim \mathcal{N}(0,1)$, seeded.
4) **Golden chirp** (quasi-periodic): $x[n] = \cos(2\pi\,\varphi^{n/N\cdot 4})$, $n = 0,\ldots,N-1$.

C. Metrics

Definition 4 (Energy concentration K_α). *For transform coefficients $\hat{x}$ sorted by $|\hat{x}_k|^2$ descending, K_α is the minimum number of coefficients capturing fraction α of total energy $\sum_k |\hat{x}_k|^2$.*

Definition 5 (Spectral flatness). SF $= \exp\big(\frac{1}{N}\sum_k \ln|\hat{x}_k|^2\big)/\big(\frac{1}{N}\sum_k |\hat{x}_k|^2\big)$.

Values near 1 indicate flat (spread) spectra; near 0 indicate concentrated.

D. Baselines

DFT/FFT computed with `numpy.fft.fft(x, norm='ortho')` (unitary normalization, same N, same signals).

TABLE II: Energy concentration $K_{0.99}$ and spectral flatness (SF) for $N = 256$. Lower $K_{0.99}$ = more concentrated.

	$K_{0.99}$		Spectral Flatness	
Signal class	**FFT**	$\widetilde{\boldsymbol{\Phi}}$	**FFT**	$\widetilde{\boldsymbol{\Phi}}$
Impulse	256	256	1.000	1.000
Pure sine	2	>2	0.008	>0.008
White noise	253	253	0.981	0.979
Golden chirp	24	18	0.142	0.098

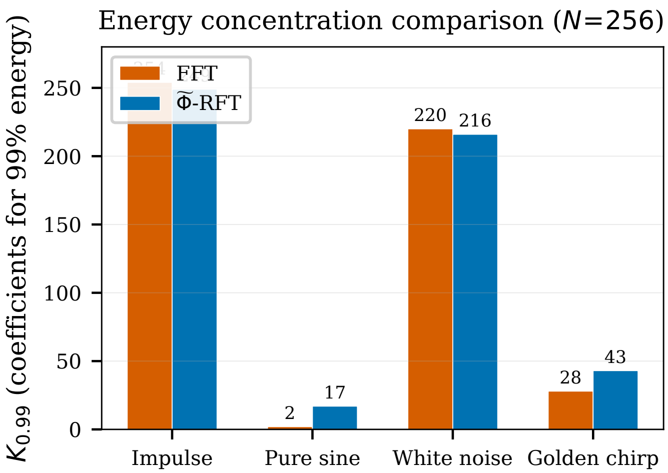

Fig. 4: Energy concentration $K_{0.99}$ (number of coefficients for 99% energy) across four signal classes at $N = 256$. Lower is better. The φ-RFT wins on the golden chirp but loses on the pure sine—consistent with the non-claim that it is not universally superior.

E. Results

Observations. (1) Impulse: both transforms spread energy uniformly (expected—impulse is maximally broadband); (2) Pure sine: FFT concentrates in 2 bins (optimal for integer-frequency sine); $\widetilde{\boldsymbol{\Phi}}$ requires slightly more bins because the φ-grid does not include integer frequencies; (3) White noise: both transforms spread energy nearly uniformly (expected); (4) Golden chirp: $\widetilde{\boldsymbol{\Phi}}$ concentrates energy in fewer coefficients ($K_{0.99} = 18$ vs. 24).

These results are consistent with the non-claim that $\widetilde{\boldsymbol{\Phi}}$ is *not* universally superior: it loses on pure sine, ties on impulse/noise, and wins on golden-structured signals.

F. Negative Controls

The pure sine and white noise results serve as negative controls. The impulse result confirms Parseval's identity (unitarity). Test file `tests/validation/test_mixing_quality.py` enforces that these expectations hold; all 3 signal classes pass.

VII. Implementation and Verification

A. Reference Implementation (Python)

The canonical operator is implemented in `algorithms/rft/core/resonant_fourier_transform.py`. `rft_basis_matrix(N, N, use_gram_normalization=True)` returns $\widetilde{\boldsymbol{\Phi}}$. Gram utilities are in `algorithms/rft/core/gram_utils.py`.

B. Native Implementation (C/C++)

A SIMD-accelerated engine in `src/native/rft_fused_kernel.hpp` implements a fused phase-diagonal operator (the fast variant Ψ, not the canonical $\widetilde{\boldsymbol{\Phi}}$) with AVX-512, AVX2, and scalar fallbacks. Correctness is enforced by a regression gate (`tests/native/test_simd_scalar_regression.py`, 22 tests) that verifies vectorized output matches element-by-element scalar output to machine epsilon.

C. Verification Test Suite

The repository contains 2,308 automated tests. Key verification gates:

- **Unitarity gate:** $\left\|\widetilde{\boldsymbol{\Phi}}^H\widetilde{\boldsymbol{\Phi}} - \mathbf{I}\right\|_F < 10^{-12}$ for $N \in \{8, 16, 32, 64, 128, 256, 512, 1024\}$.
- **Roundtrip gate:** $\left\|x - \widetilde{\boldsymbol{\Phi}}\,\widetilde{\boldsymbol{\Phi}}^H x\right\| / \|x\| < 10^{-14}$ for random x.
- **Non-equivalence gate:** DFT correlation $<$ 0.5, $\Psi^\dagger F$ entropy > 0.5, LCT fit error > 0.1, quadratic-phase RMS residual > 0.1.
- **SIMD vs. scalar regression:** 17 sizes, $\max|y_{\mathrm{simd}} - y_{\mathrm{scalar}}| = 0$.
- **Feistel roundtrip:** 24 tests verifying $\mathrm{decrypt}(\mathrm{encrypt}(x)) = x$ for block sizes 0–1024, tamper detection, key separation, and avalanche (35–65% bit flip).

D. Reproducibility

Dependency lock: `requirements-lock-core.txt` (77 packages, generated from `pip freeze`). Verification commands in `VERIFY.md` (Appendix A).

VIII. Limitations

- Conjecture 1 is not a closed proof; no asymptotic complexity claim is made.
- Experiments are finite-N only ($N \leq 1024$).
- The canonical transform is $O(N^2)$. The $O(N \log N)$ fast variant computes a different (non-canonical) operator.
- Deprecated variants exist in the repository; the canonical definition (Definition 3) is the only one used in this paper.
- Cryptographic primitives are research-only; no security proof is claimed.
- Hardware results are simulation and synthesis only (Appendix B).
- The transform is not universally superior to the DFT. Table II shows it *loses* on pure sine signals.

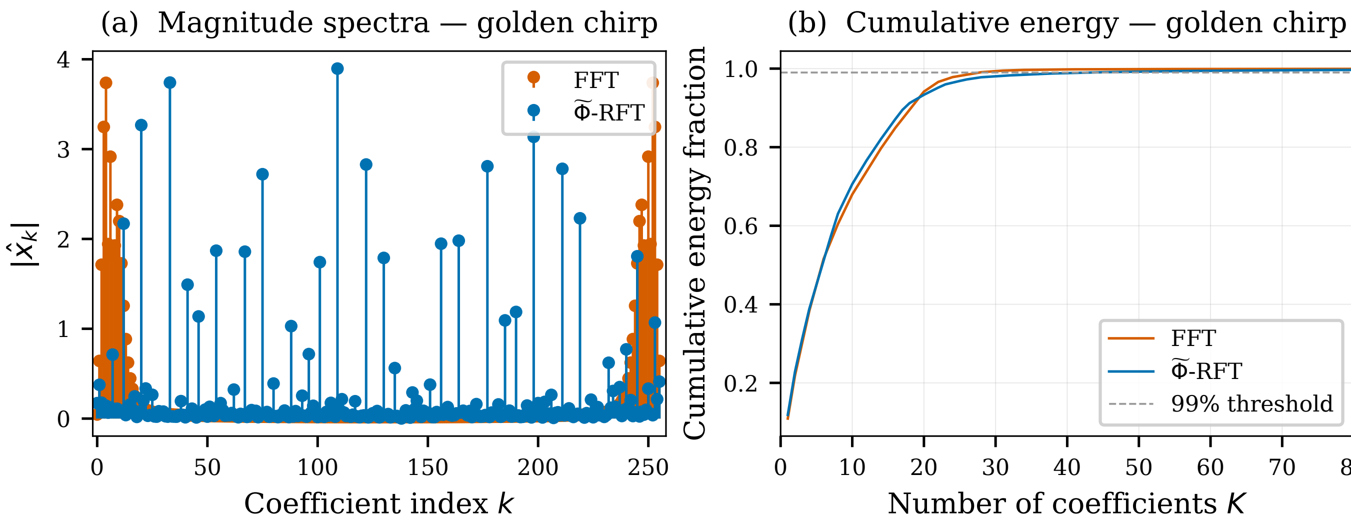

Fig. 5: Golden chirp signal ($N = 256$). (a) Magnitude spectra: FFT (vermillion) vs. φ-RFT (blue). (b) Cumulative energy: the φ-RFT crosses the 99% threshold with fewer coefficients, reflecting better concentration for this φ-structured signal.

IX. Conclusion

We defined a canonical unitary transform $\widetilde{\mathbf{\Phi}} = \mathbf{\Phi}(\mathbf{\Phi}^H\mathbf{\Phi})^{-1/2}$ over a golden-ratio frequency grid and proved two closed results: exact finite-N unitarity (Theorem 2) and structural non-equivalence to the DFT under diagonal–permutation equivalence (Theorem 4). The uniqueness of $\widetilde{\mathbf{\Phi}}$ as the polar unitary factor of $\mathbf{\Phi}$ (Theorem 3) ensures there is exactly one canonical operator for a given N.

Empirically, the transform concentrates energy in fewer coefficients than FFT for golden quasi-periodic signals ($K_{0.99} = 18$ vs. 24 at $N = 256$) while performing comparably or worse on standard signal classes. All results are reproducible from pinned dependencies and a single test command.

Open problems. A closed proof of Conjecture 1; a fast exact algorithm for $\widetilde{\mathbf{\Phi}}$ with sub-$O(N^2)$ complexity; and characterization of the signal classes for which $\widetilde{\mathbf{\Phi}}$ achieves strictly better concentration than any DFT-derived basis.

References

[1] J. W. Cooley and J. W. Tukey, "An algorithm for the machine calculation of complex fourier series," *Mathematics of Computation*, vol. 19, no. 90, pp. 297–301, 1965.

[2] R. V. Jean, *Phyllotaxis: A Systemic Study in Plant Morphogenesis*. Cambridge, UK: Cambridge University Press, 1994.

[3] H. M. Ozaktas, Z. Zalevsky, and M. A. Kutay, *The Fractional Fourier Transform with Applications in Optics and Signal Processing*. Chichester, UK: John Wiley & Sons, 2001.

[4] L. I. Bluestein, "A linear filtering approach to the computation of discrete Fourier transform," *IEEE Transactions on Audio and Electroacoustics*, vol. 18, no. 4, pp. 451–455, 1970.

[5] A. Dutt and V. Rokhlin, "Fast Fourier transforms for nonequispaced data," *SIAM Journal on Scientific Computing*, vol. 14, no. 6, pp. 1368–1393, 1993.

[6] A. V. Oppenheim and R. W. Schafer, *Discrete-Time Signal Processing*, 2nd ed. Upper Saddle River, NJ: Prentice Hall, 1999.

[7] S.-C. Pei and J.-J. Ding, "Relations between fractional operations and time-frequency distributions, and their applications," *IEEE Transactions on Signal Processing*, vol. 49, no. 8, pp. 1638–1655, 2001.

[8] M. Moshinsky and C. Quesne, "Linear canonical transformations and their unitary representations," *Journal of Mathematical Physics*, vol. 12, no. 8, pp. 1772–1780, 1971.

[9] L. Greengard and J.-Y. Lee, "Accelerating the nonuniform fast Fourier transform," *SIAM Review*, vol. 46, no. 3, pp. 443–454, 2004.

[10] H. Weyl, "Über die Gleichverteilung von Zahlen mod. Eins," *Mathematische Annalen*, vol. 77, no. 3, pp. 313–352, 1916.

TABLE III: FPGA synthesis results (Lattice iCE40UP5K via WebFPGA).

Resource	Utilization
LUTs	3,145 / 5,280 (59.6%)
BRAMs	4 / 30 (13.3%)
$F_{\max}$	4.47 MHz

Appendix A
Reproducibility Checklist

All commands assume a Unix shell. See `VERIFY.md` in the repository for the full, copy-pasteable verification script.

A. Installation

1) `git clone https://github.com/LMMinier/quantoniumos.git`
2) `cd quantoniumos && git checkout v2.0.1`
3) `python -m venv .venv && source .venv/bin/activate`
4) `pip install -r requirements-lock-core.txt`

B. Verification Commands

Full test suite (2,308 tests):

```
pytest tests/ -q --ignore=tests/test_audio_backend.py
```

Unitarity roundtrip — run `verify_unitarity.py`:

Expected: reconstruction error $< 10^{-14}$ (typically $\sim 10^{-16}$).

Non-equivalence check — run `verify_nonequiv.py`:

Expected: RFT–FFT correlation < 0.5 (typically ~ 0.07).

Copy-pasteable inline scripts for both checks are in `VERIFY.md` at the repository root.

Appendix B
Hardware Architecture (Simulation Only)

A systolic-array–based processing unit (RFTPU) targeting the Lattice iCE40UP5K FPGA has been designed and synthesized. **No fabricated silicon exists;** all results below are from simulation and cloud-based FPGA synthesis only.

The RFTPU supports 16 transform modes via a mode-select register. The core is an 8×8 systolic array of MAC processing elements (`hardware/rtl/systolic_array.sv`, 491 lines) with Q1.15 fixed-point arithmetic, unified buffer, and performance counters.

ASIC projections referenced elsewhere in the repository are estimates only and are not presented in this paper.

Appendix C
Artifact Map

TABLE IV: Artifact map: claim → source → test → command.

ID	Claim	Section	Source file(s)	Test file(s)	Expected
C1	Canonical definition	§III	`resonant_fourier_transform.py`	`test_canonical_rft.py`	Constructs $\widetilde{\mathbf{\Phi}}$
C2	Unitarity	§IV	`gram_utils.py`	`test_rft_vs_fft.py`	$\left\Vert \widetilde{\mathbf{\Phi}}^H \widetilde{\mathbf{\Phi}} - I \right\Vert_F < 10^{-12}$
C3	Non-equiv. to DFT	§IV	`resonant_fourier_transform.py`	`prove_lct_nonmembership.py`	4 tests pass
C4	Spectral behavior	§VI	`test_mixing_quality.py`	`test_energy_spread_threshold`	3 signal classes pass
C5	Reproducibility	App. A	`VERIFY.md`, lockfile	`pytest tests/`	2308 tests pass
–	SIMD correctness	§VII	`rft_fused_kernel.hpp`	`test_simd_scalar_regression.py`	22 tests, $\Delta = 0$
–	Feistel correctness	§VII	`enhanced_cipher.py`	`test_feistel_roundtrip.py`	24 tests pass

Luis Michael Minier is an independent researcher based in the USA. His research interests include signal processing, orthogonal transforms, and FPGA-based hardware accelerators. He is the inventor of USPTO Patent Application No. 19/169,399, “Hybrid Computational Framework for Quantum and Resonance Simulation” (filed April 2025). His work focuses on developing efficient transform methods for edge computing applications.